Acta Oceanol. Sin., 2021, Vol. 40, No. 8, P. 78–88
https://doi.org/10.1007/s13131-021-1803-5
http://www.aosocean.com
E-mail: ocean2@hyxb.org.cn

The influence of coupling mode of methane leakage and debris input on anaerobic oxidation of methane

Rui Xie[1, 2, 3], Daidai Wu[1, 3, 4*], Jie Liu[1], Guangrong Jin[1], Tiantian Sun[1], Lihua Liu[1], Nengyou Wu[4, 5]

[1] Key Laboratory of Gas Hydrate, Guangzhou Institute of Energy Conversion, Chinese Academy of Sciences, Guangzhou 510640, China

[2] Guangzhou Marine Geological Survey, China Geological Survey, Ministry of Natural Resources, Guangzhou 510075, China

[3] Institution of South China Sea Ecology and Environmental Engineering, Chinese Academy of Sciences, Guangzhou 510301, China

[4] Evaluation and Detection Technology Laboratory of Marine Mineral Resources, Pilot National Laboratory for Marine Science and Technology (Qingdao), Qingdao 266237, China

[5] Key laboratory of Gas Hydrate, Ministry of Natural Resources, Qingdao 266071, China

Received 6 July 2020; accepted 9 December 2020

Abstract

Anaerobic oxidation of methane (AOM) is an important biogeochemical process, which has important scientific significance for global climate change and atmospheric evolution. This research examined the $\delta^{34}S$, terrigenous clastic indices of TiO_2 and Al_2O_3, and times for formation of the Ba front at site SH1, site SH3 and site 973-4 in the South China Sea. Three different coupling mechanisms of deposition rate and methane flux were discovered. The different coupling mechanisms had different effects on the role of AOM. At site 973-4, a high deposition rate caused a rapid vertical downward migration of the sulphate–methane transition zone (SMTZ), and the higher input resulted in mineral dissolution. At site SH3, the deposition rate and methane flux were basically in balance, so the SMTZ and paleo-SMTZ were the most stable of any site, and these were in a slow process of migration. At site SH1, the methane flux dominated the coupled mode, so the movement of the SMTZ at site SH1 was consistent with the general understanding. Understanding the factors influencing the SMTZ is important for understanding the early diagenesis process.

Key words: methane seep, terrestrial detrital material, anaerobic oxidation of methane, gas hydrate

Citation: Xie Rui, Wu Daidai, Liu Jie, Jin Guangrong, Sun Tiantian, Liu Lihua, Wu Nengyou. 2021. The influence of coupling mode of methane leakage and debris input on anaerobic oxidation of methane. Acta Oceanologica Sinica, 40(8): 78–88, doi: 10.1007/s13131-021-1803-5

1 Introduction

Methane is an important greenhouse gas in the atmosphere, and its greenhouse effect is 25 times that of CO_2. The concentration of methane in the atmosphere has increased by 150% since 1975 and continues to grow at a rate of 1.0%–1.2% per year (Kotelnikova, 2002). The ocean is the largest methane reservoir on the planet. It is estimated that about 5 000 Gt (according to carbon) of methane is contained in oceanic anaerobic sediments. Most of this methane (3 000 Gt (according to carbon)) is consolidated in hydrates, but 2 000 Gt (according to carbon) is stored as free gas (Dong et al, 2019). Although there is a large amount of methane in the ocean, the ocean contributes only 2% to the methane in the atmosphere. In 1992, the Intergovernmental Panel on Climate Change (IPCC) pointed out that the actual amount of methane produced in marine sediments is much higher than the annual methane content released into the atmosphere by the ocean. Research has shown that the methane produced by marine sediments is almost completely consumed by anaerobic oxidation of methane (AOM) and that 90% of this methane is consumed by anaerobic microorganisms in anoxic sediments (Wankel et al, 2012; Lloyd et al, 2006).

In the South China Sea (SCS), many studies have examined the relationship between methane leakage and AOM and also the operational mechanism of AOM (Li et al, 2008; Tong et al, 2013; Feng and Chen, 2015; Zhang et al, 2017). Wu et al (2011) studied the change of sulphate and methane concentrations in the pore water and indicated that the sulphate–methane transition zone (SMTZ) in the Shenhu area is basically around 20 m depth, which is generally consistent with the internationally common SMTZ of 10–50 m, indicating moderate leaking of methane in the northern part of the SCS. Li et al, (2017) considered that the flux of methane leakage has an important influence on the SMTZ in sediment. When the methane leakage flux is large, the SMTZ in the sediment is relatively shallow; and when the methane leakage is small, the SMTZ in the sediment is relatively deep. Therefore, the depth of the SMTZ in sediment can be used as an indicator of bottom methane leakage. Meanwhile, the SMTZ is also the sedimentary interval where methane driven authigenetic carbonate

Foundation item: The Guangdong Basic and Applied Basic Research Fund Project under contract No. 2021A1515011509; the Municipal Science and Technology Program of Guangzhou under contract No. 201904010311; the Special Project for Marine Economy Development of Guangdong Province under contract No. GDME-2018D002.
*Corresponding author, E-mail: wudd@ms.giec.ac.cn

(MDAC) precipitates (Eq. (1)). AOM elevates porewater alkalinity (Egger et al, 2015) and thus promotes the precipitation of $Ca(Mg/Sr)CO_3$ (Eq. (1)):

$$2HCO_3^- + Ca^{2+}\left(\frac{Mg^{2+}}{Sr^{2+}}\right) \rightarrow Ca(Mg/Sr)CO_3 + CO_2 + H_2O. \quad (1)$$

The MDAC is often aragonite and high-Mg calcite (Feng and Chen, 2015; Zhang et al, 2018a), and it provides direct geological evidence of AOM and methane seepage in the sedimentary record (Panieri et al, 2017). The $\delta^{13}C$ value of the carbonate formed in the SMTZ layer is generally consistent with the value of the organic gas. Carbonates with $\delta^{13}C$ values less than –30‰ Vienna Pee Dee Belemnite (VPDB) are generally consistent with carbon sourced from gas hydrate. At the same time, who studied pore water and pyrite values of $\delta^{34}S$ in the northern SCS, found that AOM results in a positive deviation of $\delta^{34}S$. During AOM, sulphate is usually consumed under semi-closed or closed conditions, as reflected in ^{34}S-enriched sulfide minerals (Egger et al, 2016). The results showed extreme variability in $\delta^{34}S$ values, ranging from –51.3‰ to 114.8‰ (Wankel et al, 2012; Egger et al, 2016). In methane-rich environments, the ^{34}S–^{32}S fractionation of AOM is usually smaller than 40‰.

In addition, the debris input also caused the change of SMTZ (Lin et al, 2018). The influencing factors leading to the change of SMTZ depth are mainly related to non-steady state (non-steady state) deposition and/or fluid events. On the one hand, the appearance of landslide, slump and rapid deposition will trigger the denudation, transportation and redeposition of sediments, which will change the original steady state of geochemical conditions and sediments conditions (Liu et al., 2019).

Although Liu et al (2018) has found vivianite below the SMTZ at site 973-4 and considered that vivianite be influenced by the metal-driven anaerobic oxidation of methane. And later, Wu et al (2020) also found the evidence of metal-driven anaerobic oxidation of methane at site 973-4. Zhang et al (2018a) found the difference distribution of foraminifera at site 973-4. Zhang et al (2018b) interpreted the elemental Fe-P-S cycles at site 973-4, there are few studies have examined the relationship between the input of terrestrial debris (TD) and the relationship and AOM. In general, the total fluvial sediment discharge into the modern SCS is large, amounting to 8.4% of the total input into the global oceans, making the SCS the largest sink of fluvial sediments among the enclosed or semi-enclosed marginal seas of the world (Liu et al, 2016; Zhao et al, 2017; Zheng et al, 2018). Therefore, studying the relationship between sediment input and AOM is a good method for understanding sedimentary evolution and methane leakage. In this paper, the following scientific problems are addressed: (1) the influence of land source debris input on AOM and (2) the performance characteristics of AOM in different geological environments.

2 Geological setting

The SCS is located at the intersection of the Eurasian Plate, Pacific Plate, and Indian Plate and is one of the largest marginal seas in the western Pacific (Liu and He, 2001). The northwestern part of the SCS is a typical passive continental margin, and the northeastern part has an active convergent continental margin (Yao, 1996). After the Middle Miocene, a regional sedimentary layer dominated by marine sediments developed on the continental slopes in the northern part of the SCS (Wu et al, 2009). From west to east, these deposits formed in the Qiongdongnan Basin, Zhujiang River Mouth Basin, and Tainan Basin (Feng et al, 2018).

The Shenhu area, including the area east of the unified shoal, is located in the middle of the southern slope of the SCS, that is, the sea between the Xisha Trough and the Dongsha Islands (Fig. 1). The geological structure is part of the Baiyun Sag of the Zhujiang Depression in the Zhujiang River Mouth Basin (Wu et al, 2009). The water depth of the study area, which is the transition zone between the northern slope of the SCS and the central basin, is 1 000–3 000 m below the sea surface (Fig. 1). The sedimentation rate is high, and the sedimentary thickness of the Cenozoic deposits is 1 000–7 000 m. The organic carbon in the thick sediments is dominantly within marine facies with contents of 0.2% to 1.9% (Su et al, 2012). The organic matter content is lower in the shallow layers and relatively higher in the deep layers. The Shenhu area is one of the most active areas of tectonic movement in the northern part of the SCS. Cenozoic faulting is extremely well developed. The NW-trending faults of the Late Miocene can extend down to Palaeogene strata, providing a channel for deep fluid migration to higher levels, and the shallow portion is widely penetrated by a large number of NE-trending faults, which may facilitate further migration of hydrocarbon-bearing fluids to small faults (Su et al, 2016). In addition, the sea area has a well-developed diapiric structure, and gas leakage is very strong, which also affects gas hydrate accumulation (Wu et al, 2009).

The seabed topography of the Taixinan Basin is inclined from the northwest to the southeast. In the northwestern shelf transition zone and the upper land slope, the seabed topography and slope change greatly. To the southeast, the water depth increases slowly, and the topography is relatively flat. The topography of the seabed in the study area is complex, and the slope angle changes greatly. The upper slope is steep, but the lower slope is gentle. Three levels of geomorphic units, submarine canyons, land slopes, and seabed slopes, can be distinguished. Descending steps of the terrain and steep slopes, terraces, erosional valleys, sea hills, sea valleys, scoured trenches, landslides, seamounts, and other secondary landform types can be identified (Zhang et al, 2002, 2013; Wang et al, 2015). A dense series of NE-trending normal faults is developed in the study area and forms gas migration channels with associated gas chimney structure, which is conducive to the formation and development of hydrates. Miocene turbidites are well developed in the study area. The Pliocene is dominated by canyon, natural dyke, and semi-oceanic deposits.

3 Methods and samples

3.1 *Samples*

The site SH3 and site SH1 samples used in this study were obtained by the Guangzhou Marine Geological Survey in the Shenhu area of the SCS in 2007 (Su et al, 2015). Site SH3 is of particular interest because of its high hydrate saturation and thicker hydrate-bearing sediments. The sediments are mainly muddy but include silt with clay or sand as a secondary component. In this study, 31 samples were obtained from site SH3 from 0–25 m below seafloor, and the main trace elements were measured separately. And the site SH1 is very closed to the site SH3. At site SH1, the sediments are same as site SH3. However, there is no gas hydrate in sediments. In this paper, 11 samples collected from the site SH1. The $\delta^{34}S$ values, main and trace elements were measured separately.

Core 973-4 has four distinctive lithological intervals, as summarised from Wang (2013). The sediments in the intervals of 12–450 cm and 450–530 cm are composed of celadon silty clay and grey clayey silt, respectively. The 530–603 cm interval con-

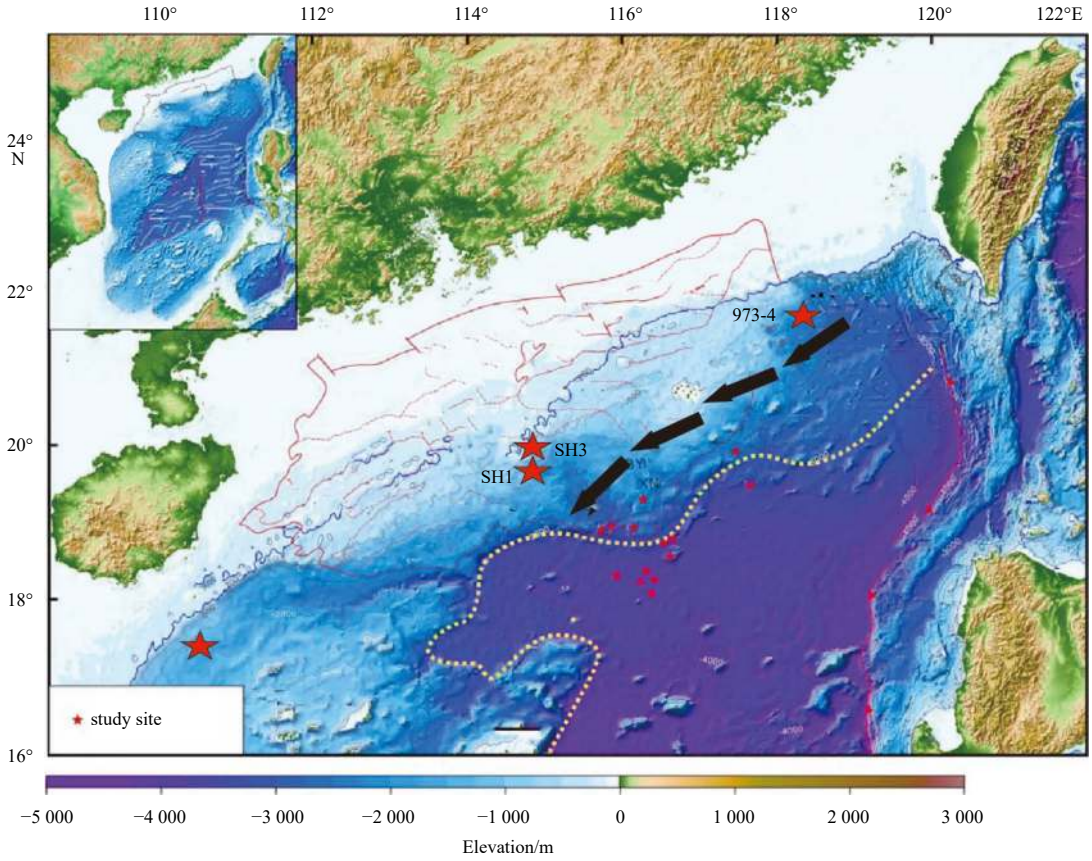

Fig. 1. Locations of sites SH3, SH1 and 973-4 (the red five-pointed star in the picture). The black arrows show the direction of bottom flow in the northern part of the South China Sea.

sists of celadon clayey silt with abundant foraminiferal shells. The 603–1 375 cm interval consists of grey silty clay with patchy hydrogen-sulphide textures (Zhang et al, 2018b). In this study, we selected 64 samples from site 973-4 and conducted analytical tests.

3.2 *Major and trace element measurements*

Major elements in the sediments were analysed at the Analytical and Testing Center of the Guangzhou Institute of Energy Conversion, Chinese Academy of Sciences. X-Ray fluoresccene spectrometry (XRF; Thermo ARL ADVANTta IntelliPowerTM 2000, Waltham, MA, USA) was used to determine the primary element contents. The measured XRF spectral data were converted to elemental and oxide contents using UniQuant semi-quantitative analysis software. The whole rock trace element contents were analysed using an inductively coupled plasma mass spectrometer (ICP-MS; Agilent 7700e, Santa Clara, CA, USA) at the analysis and testing centre of the Wuhan Shangpu Analysis Technology Co., Ltd.

Total organic carbon (TOC) was measured using a Heraeus (Ulm, Germany) CHN-O Rapid Elemental Analyzer. Before testing, the appropriate sediments were selected, excess calcium carbonate was removed by adding 10% HCl, and the sample was diluted several times with distilled water before being placed in an oven at 50°C. The TOC test instrument accuracy was greater than 1%. The aforementioned experimental process was conducted at the Guangzhou Institute of Geochemistry, Chinese Academy of Sciences. Total sulphur and total carbon tests were performed using an element analyser (Vario EL cube; Elementar, Alb-Donau-Kreis, Germany) with an accuracy of 0.1%. To burn and decompose it, the rock powder sample was oxidised catalytically in oxygen at a high temperature, producing a mixture containing C and S gases. These mixed gases were then placed into contact with tungsten oxide and copper to convert them into CO_2 and SO_2 gases, at which point the sample was separated by a column. A thermal conductivity detector was used to calculate the C and S component contents by comparing the test sample with a standard sample. The aforementioned pretreatment and experimental procedures were completed at the Analytical Testing Center of the Guangzhou Institute of Energy Research, Chinese Academy of Sciences.

3.3 *Determination of $\delta^{34}S$*

Reduced inorganic sulphur (RIS) in the samples was extracted using $CrCl_2$ and HCl. This reduction method can release sulphur contained in all sulphide lattices, so the obtained sulphur content was almost equal to the total content of chromium reducible sulphur (CRS). The reduced sulphur was converted to H_2S gas, which was blown out by the carrier gas (nitrogen), and then precipitated by passing it through an $AgNO_3$–NH_3H_2O solution to obtain silver sulphide. The silver sulphide was filtered, dried, and weighed. Then, the weight percentage of CRS in the deposit was calculated according to the weight of precipitated silver sulphide. The detailed experimental steps can be found in Panieri et al (2017).

During the experiment, quantitative addition of pyrite as a

standard sample resulted in a recovery rate of 88%–92%. The silver sulphide was then sent to the State Key Laboratory of Biogeology and Environmental Geology of China University of Geosciences (Wuhan, China) for analysis of $\delta^{34}S$ using an elemental analysis–isotope ratio mass spectrometer (Delta V Plus). All results were reported in standard delta notation as per mil deviations from the Vienna-defined Canyon Diablo Troilite (VCDT). The standard deviation of the measurements was less than 0.2‰ (VCDT). Measurement errors of about 0.2‰ (1σ) were calculated from replicate analyses of the IAEA international standards IAEA S1 (–0.3‰), IAEA S2 (+22.7‰), and IAEA S3 (–32.3‰).

4 Results

4.1 *The main and trace element characteristics at sites 973-4, SH1 and SH3*

At site 973-4, all the data changed dramatically at 400–600 cm below seafloor. Among them, MgO and SrO showed opposite trends. The indicators of primary productivity of Cu/Al and Ni/Al show the same trend of change and both decrease rapidly at 400–600 cm below seafloor. The changing trends of U and Mo show opposite trends. However, at site SH3, there are two obviouly change of main and trace element at 7–15 m below seafloor and 17.5–20 m below seafloor, all the data have increased invariably. But the study found that all mineral indicators have a greater increase at 8–15 m below seafloor than at 17.5–22 m below seafloor. The main changes at site SH1 in the 25–36 m below seafloor position. In the 25–36 m below seafloor, all the data declined.

4.2 *The characteristics of $\delta^{34}S$ at sites 973-4, SH1 and SH3*

At site SH3, the $\delta^{34}S$ values increase from –49‰ to –35‰ at 10–15 m below seafloor, and later, the $\delta^{34}S$ values increase from –35‰ to –11‰ at 17.5–20 m below seafloor. At site SH1, the $\delta^{34}S$ values increase at 25–36 m below seafloor. At site 973-4, the $\delta^{34}S$ increase from –40‰ to 10‰ at 650–900 cm below seafloor.

5 Discussion

5.1 *Evidence of anaerobic oxidation of methane and its movement*

Generally, in oxic and suboxic sediments, reduced sulphur and organic carbon contents show a correlation with an average S/C ratio of 0.36 (Berner, 1981; Li et al, 2016a, 2016b) (Fig. 2). In euxinic sediments, similar to those of the Black Sea, the S/C ratio is always higher than 2.05 (Leventhal, 1983). Moreover, in methane-rich sediments, where AOM is the predominant process, AOM-induced pyrite formation may increase the S/C ratio of sediments (Lim et al, 2011; Sato et al, 2012). At site SH3, the S/C ratio of the 0–8 m below seafloor interval was very close to 0.36 (Fig. 2). However, in the same layer, the U/Al and Mo/Al ratios were not enriched (Figs 3e and k), indicating an oxidising environment. This result is consistent with the S/C ratio in the oxic sediments of the Black Sea. The S/C ratios in the 8–15 m and 18–22 m below seafloor intervals were higher than 0.36 (Fig. 2). This result may indicate that there are two stages of AOM at SH3. However, at site 973-4, the S/C ratio of the 700–869 cm below seafloor interval was higher than 0.36 (Fig. 2), and the ratio was close to 0.36 at other layers of site 973-4, indicating that AOM occurs only in the 600–800 cm below seafloor interval of site 973-4 (Fig. 2).

Total sulphur (TS) and TOC showed a positive correlation in the 0–6 m below seafloor interval of site SH3, where the average S/C ratio was 0.36. The changes with depth of TiO_2, Al_2O_3, and SiO_2 were also examined. These increased significantly in the 0–6 m below seafloor depth, indicating a high land-derived input of organic matter to the sediments (Figs 4a–e). The low reactivity of land-derived organic matter and the normal oxic marine environment may account for the lower S/C ratio. At site SH3, high contents of CRS were observed in the 8–15 m and 18–22 m below seafloor intervals (Fig. 5). In these two layers, the concentration of TS increased significantly (Fig. 2); however, the TOC content remained constant, with an average of 0.35 (Fig. 2), which excluded the mechanism of additional CRS formation in a euxinic environment. The main reason for this is AOM. At the same time, high values of $\delta^{34}S$ (Fig. 5), greater than the value of average seawater sulphate $\delta^{34}S$ of 21‰, occurred in the 8–15 m and 18–22 m below seafloor intervals (Fig. 5a). Many studies have shown that a

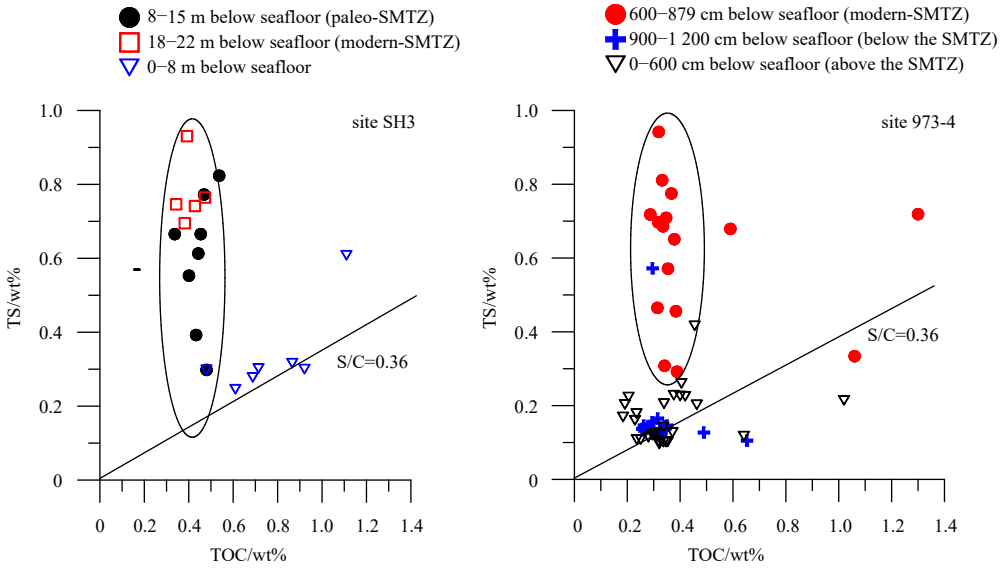

Fig. 2. Correlation between total sulphur (TS) and total organic carbon (TOC). As shown clearly in the figure, TS/TOC is significantly higher in the SMTZ.

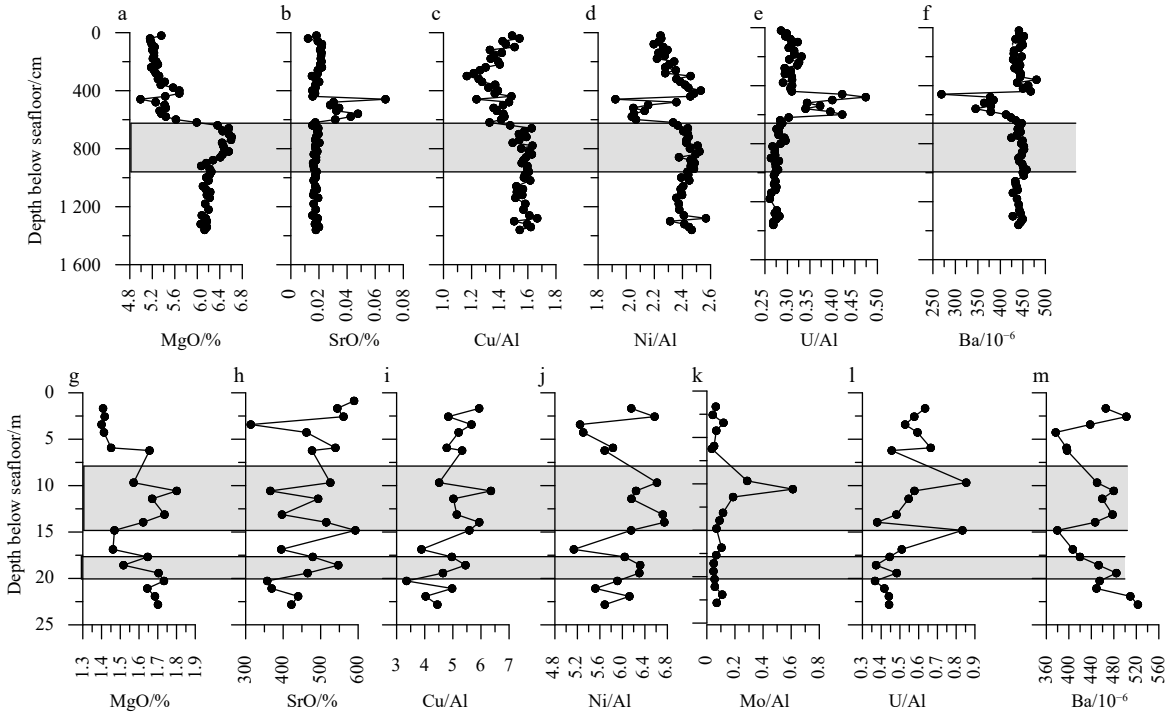

Fig. 3. Changes in elements closely related to carbonates and changes in the redox environment (U and Mo) of sites 973–4 (a–f) and SH3 (g–m).

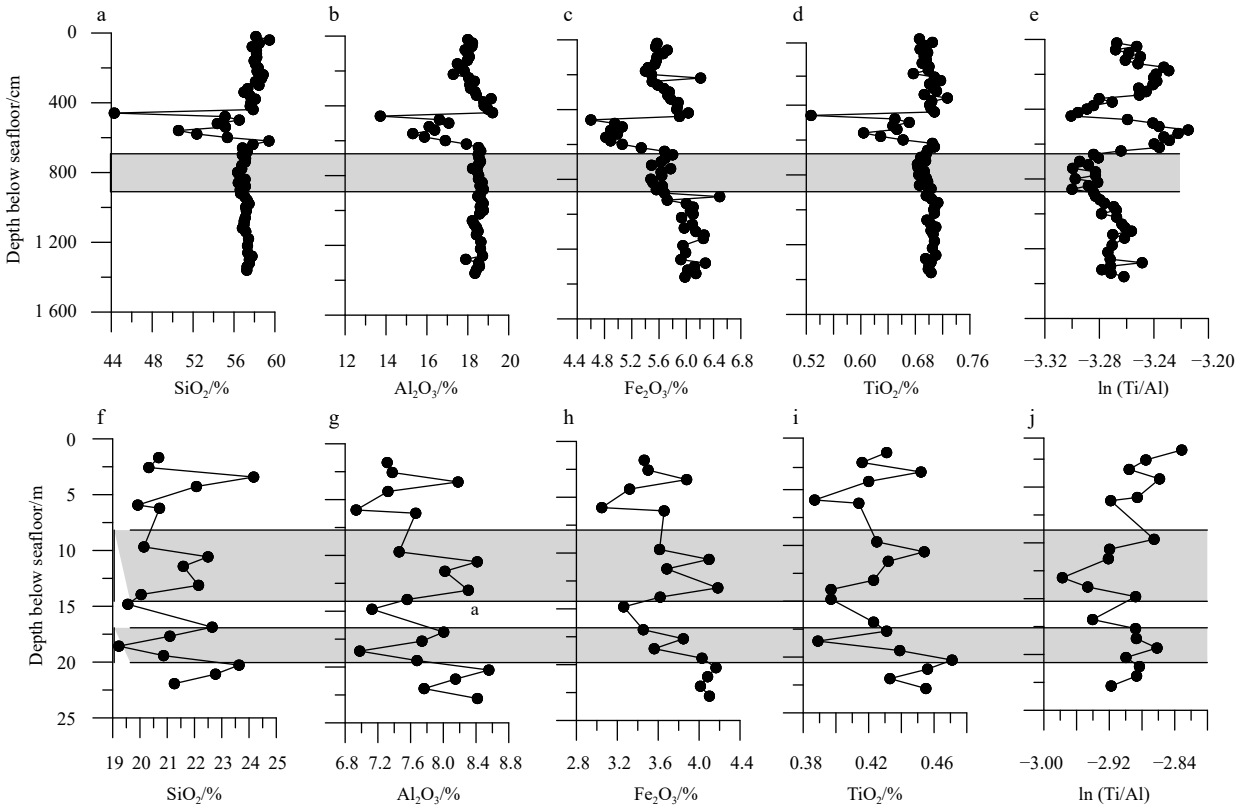

Fig. 4. Variations of land-sourced debris index values with depth at sites 973–4 (a–e) and SH3 (f–j). At the top of the SMTZ of site 973-4, all debris indicators show a downward trend.

significant positive bias of $\delta^{34}S$ indicates the occurrence of AOM (Wu et al, 2011; Egger et al, 2016; Lin et al, 2017; Zhang et al, 2018b).

As mentioned previously, the S/C ratio at site 973-4 was high-

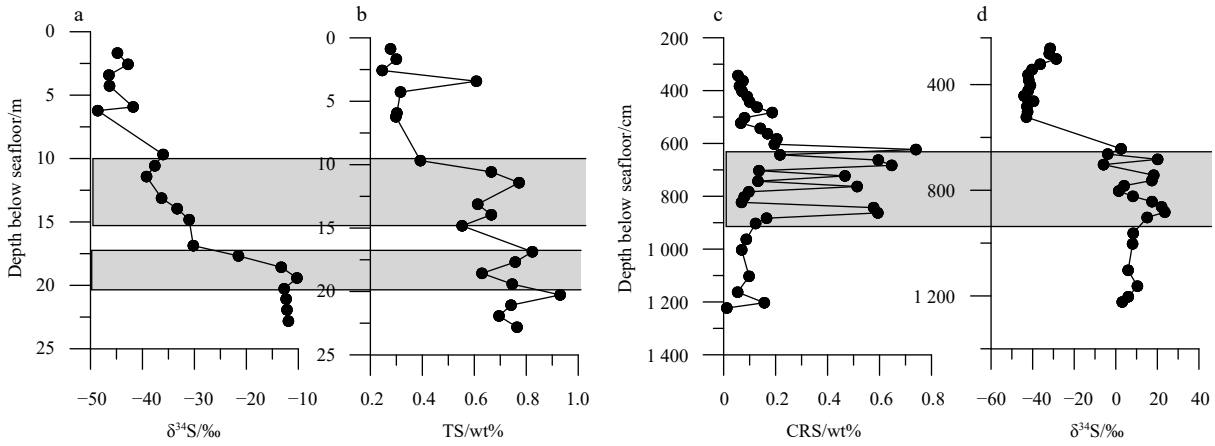

Fig. 5. Illustrations showing two periods of sudden increase of $\delta^{34}S$ in site SH3 (a,b) but only one increase of CRS and $\delta^{34}S$ in site 973-4 (c,d).

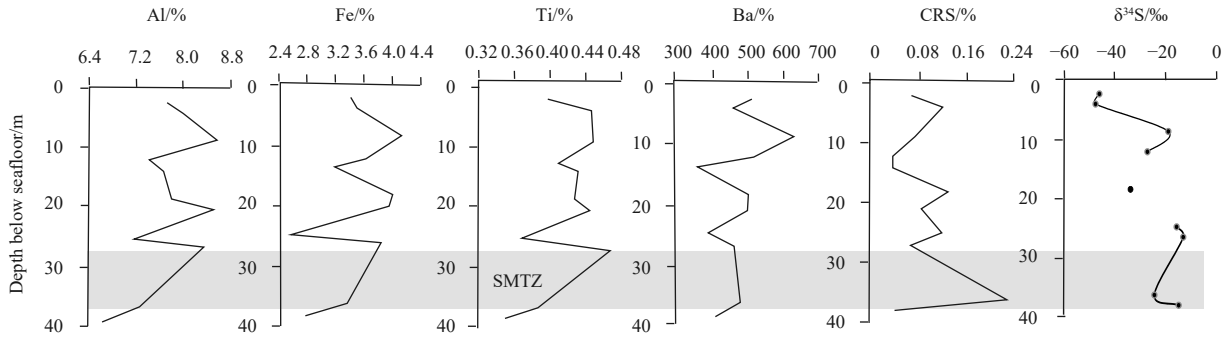

Fig. 6. Variations of land-based debris indices with depth at site SH1.

er than 0.36 in the 700–869 cm below seafloor interval and close to 0.36 in the other layers (Fig. 2). This indicates a potential AOM effect in the 700–869 cm below seafloor interval. The concentrations of TiO_2 and Al_2O_3 (Figs 4a–e) decreased at 700–890 cm below seafloor, indicating that the input of TDM was low. However, Shao et al (2007) considered that there are contour current sediments at the top of the SMTZ at site 973-4, there is no significant increase of authigenic carbonate in the modern SMTZ (600–860 cm below seafloor). At site 973-4, the study found a marked decrease in carbonate at the top of the SMTZ. The value of $\delta^{34}S$ increased obviously at 700–860 cm below seafloor. Combined these data confirm the occurrence of AOM at 700–860 cm below seafloor, the same increase trend of CRS was found at 27–37 m below seafloor at site SH1 (Fig. 6).

5.2 *Characteristics of the Ba front at sites 973-4 and SH3*

As discussed above, there are two SMTZ, at 8–15 m below seafloor and 19–25 m below seafloor, respectively, at site SH3. Moreover, high Ba concentrations (exceeding 420×10^{-6}) occur in the 8–15 m and 19–23 m below seafloor intervals. The peak Ba concentrations within these zones exceed 480×10^{-6}. The Ba fronts (defined here as intervals with Ba>430×10^{-6}) at site SH3 are diffuse, extending over several meters with multiple peaks. For example, at site SH3, a Ba front extends from 8 m to 15 m below seafloor and contains at least two peaks with Ba>430×10^{-6}. Additionally, a second Ba front was also found at the top of the current SMTZ (19–25 m below seafloor) of site SH3 (Dickens, 2001). In general, two primary components contribute to high Ba concentrations. For example, high concentrations of aluminosilicate phases and barite may increase the Ba content. The Ba from aluminosilicates is generally immobile, but the Ba hosted in barite is influenced by SO_4^{2-}. During AOM, most of the SO_4^{2-} is consumed by methane, so barite decomposes at the bottom of the SMTZ. The Ba^{2+} migrates upward until it reaches an environment rich in SO_4^{2-}, where it re-stabilises gradually. Therefore, the Ba front can help identify the position of the SMTZ. However, it is necessary to eliminate the major elements influencing the Ba fronts, and an alternative means of displaying downcore changes in sedimentary Ba content is to normalise Ba to Al (Dickens and Owen, 1996). The downcore profiles of Ba/Al at sites SH3 and 973-4 are very similar in shape to the profiles of bulk sediment Ba (Fig. 7). The similarity of the two profiles strongly suggests that the observed Ba fronts originate from digenetic accumulations of labile Ba. A double Ba peak distribution was found at the top of the SMTZ and the paleo-SMTZ, indicating instability of the paleo-SMTZ and the SMTZ through geological history and that there is a trend of vertical movement. In contrast to the Ba front at site SH3, there is a decrease in concentration of Ba at the top of the SMTZ at site 973-4. At the same time, most of the major and trace elements are lower. Shao et al (2007) considered that contour current sediments occur at the top of the SMTZ at site 973-4, and Xie et al (2019) thought that the contour current sediments caused the SMTZ to migrate downward quickly. These conclusions are consistent with the results of this study. This is the reason why there is no Ba front at the top of SMTZ. Previous studies have shown that the formation of barium sulphate in the SMTZ requires two conditions: a stable ion source and a relatively stable SMTZ position. Because the presence of an SMTZ makes the supply of Ba^{2+}

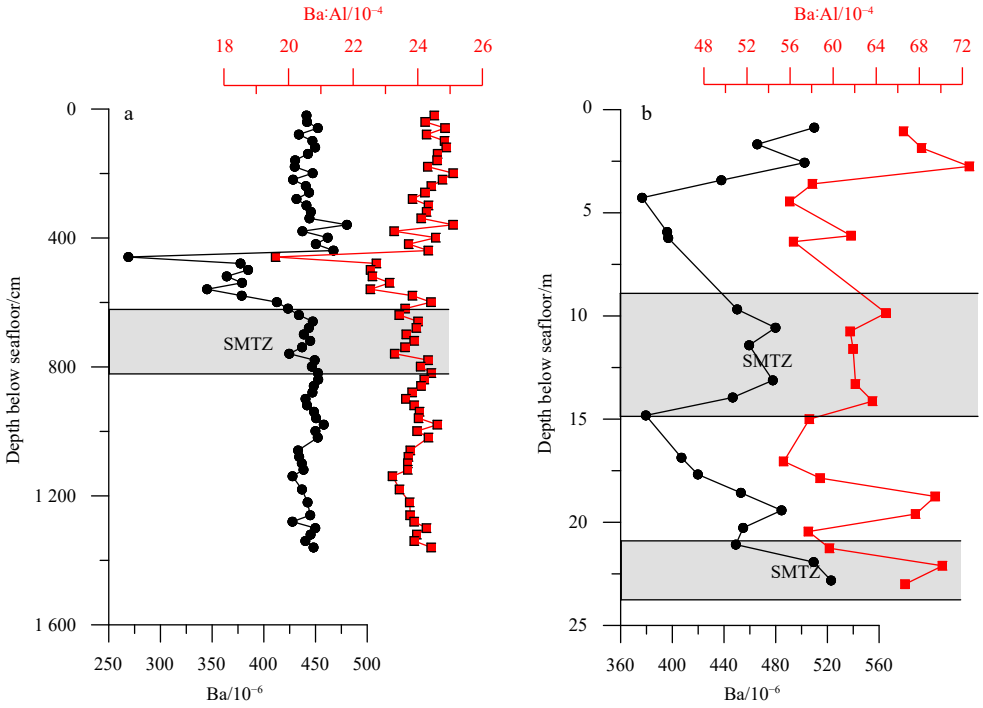

Fig. 7. Ba fronts of sites 973-4 (a) and SH3 (b).

stable and sufficient, the Ba peak in the study area is more affected by the stability of the SMTZ. Li et al (2017) considered that the movement of the SMTZ is influenced by the methane flux from the bottom sediments. When the methane flux is higher, the SMTZ is shallower; and when the methane flux is lower, the SMTZ is deeper. Lin et al (2018) found that the sedimentation rate also influences movement of the SMTZ. Therefore, to understand the movement mechanism of the SMTZ, it is necessary to compare the change in methane flux at the bottom and the change in deposition rate at the top of the SMTZ fully.

5.3 *Quantification of barium fronts and upward methane fluxes at the present and in the past*

Determining the size of the methane flux is an important process. Under normal circumstances, the SMTZ is relatively shallow when the methane flux is relatively large and is relatively deep when the methane flux is relatively small. Thus, the SMTZ can partially indicate the amount of methane flux at the bottom. Dickens (2001) also suggested that an obvious Ba front requires at least 10^4 to 10^6 years to form. However, if the methane flux is highly variable or decreases over time, a small Ba front should exist at multiple depths. At site SH3, double Ba fronts at the paleo-SMTZ and the current SMTZ are not obvious. Therefore, the methane flux from the bottom must have been variable over geological time (Dickens, 2001). In fact, sedimentary organic matter can affect the diffusion of CH_4; thus, the CH_4 diffusion flux in sediments of the study area can be calculated according to Fick's laws (Eqs (2) and (3)):

$$J = -\varphi Ds\frac{\mathrm{d}c}{\mathrm{d}x}, \tag{2}$$

where J is the diffusion rate (mmol/(m²·a)), φ is the sediment porosity, Ds is the sediment diffusion coefficient (m²/a), c is the CH_4 concentration (mmol/dm³), and x is the sediment depth (m). Ds can be defined as follows:

$$Ds = \frac{Do}{1 + n(1-\varphi)}, \tag{3}$$

where n=3 (lithology factor of silty clay) and Do=1.4×10⁻⁵ cm²/s (initial diffusion coefficient of methane at 20°C). In the Shenhu area, the average sediment porosity and grain density for sediment at site SH3 are 40% and 2.6 g/cm³, respectively (Jin et al, 2019).

According to Table 1, the methane flux at the bottom of the southwestern Taiwan Basin is significantly greater than the methane flux in the Shenhu area. However, it is strange that site 973-4 in the southwestern Taiwan Basin did not show a significant upward movement of the SMTZ due to the increase in the bottom methane flux. Instead, through a comprehensive analysis of the main trace elements and isotopes, it is believed that the SMTZ has migrated downward quickly. Analysis of sediment Mg/Ca and Sr/Ca ratios at site 973-4 (Fig. 8), site SH1, and site SH3 revealed that the sediments at site 973-4 received greater inputs of sediments than site SH1 and site SH3. Therefore, although there is certainly a high flux of methane at the bottom of

Table 1. Methane flux changes of the study area

Area	Methane flux/(mmol·m⁻²·a⁻¹)	Sulphate flux/(mmol·m⁻²·a⁻¹)	Reference
Shenhu area	0.01–4.51	/	this study
Taixinan Basin	0.01–87.0	1.01–161	Lin et al. (2006)
Black Ridge, Atlantic	7.20–7.90	7.90–8.60	Dickens (2001)

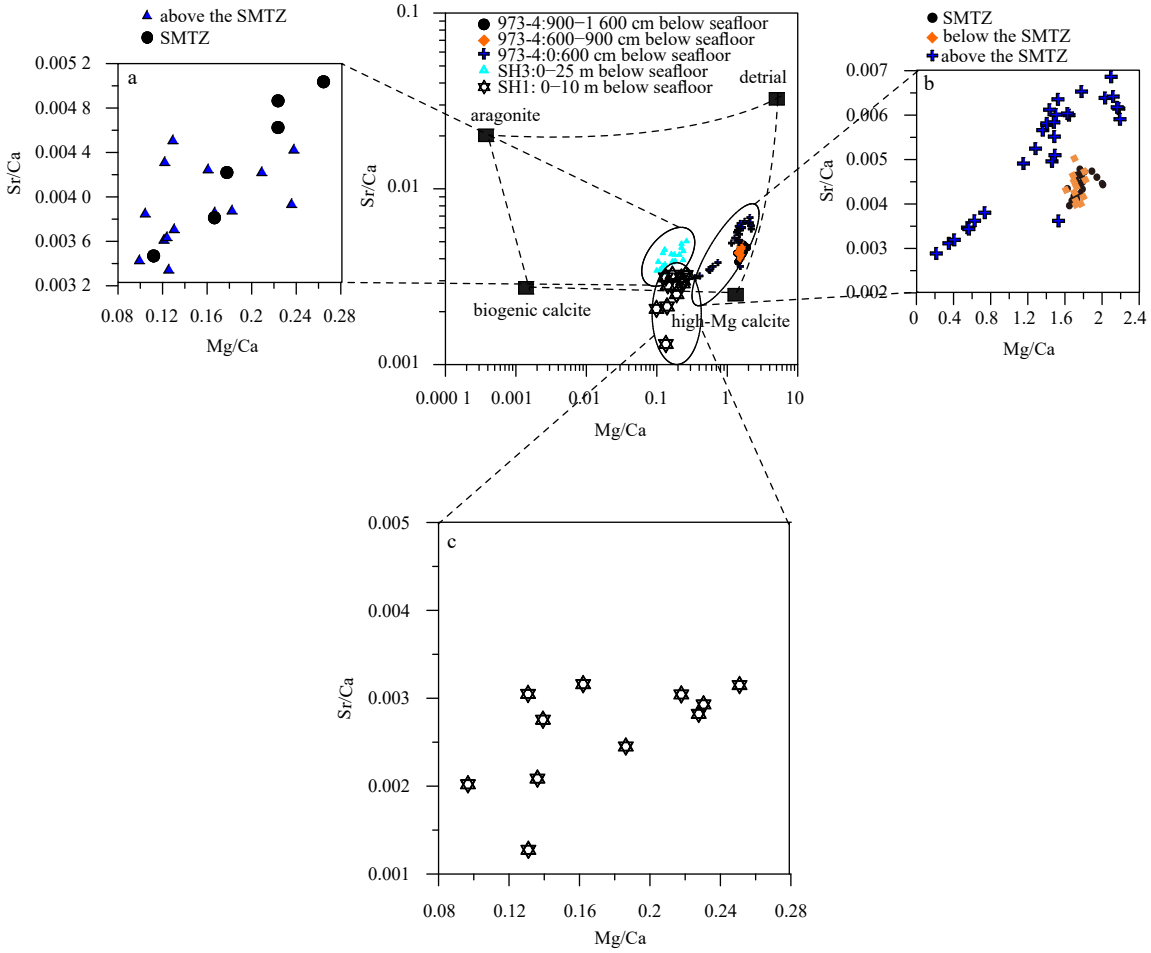

Fig. 8. Influence of the types of debris in sites SH3 (a), 973-4(b) and SH1 (c). The influence of debris input was significantly larger for site 973-4 than for site SH3.

site 973-4, the deposition rate at the top is significantly higher than the other two sites and the movement at the site is controlled mainly by changes in deposition rate. Affected by the rapid contour current sedimentation, the SMTZ at site 973-4 dropped quickly by approximately 1 m.

Site SH1 is the station least affected by debris input (Fig. 8) because Mg/Ca and Sr/Ca ratios (Fig. 8) of its sediment indicate that it has greater deposition of biological debris. Because site SH1 is very close to site SH3, the deposition rates at the top are basically the same. However, the difference is that the position of the SMTZ at site SH1 is about 10 m deeper than the current SMTZ position at site SH3. As the top deposition rate is basically the same, the main reason for the difference is the difference in bottom methane flux. During the GMGS1 voyage in 2007, hydrates were found in the 190–205 m below seafloor horizon of SH3. Hydrates are stable materials formed in a high-pressure and low-temperature environment and sometimes are susceptible to disasters such as seabed landslides. The impact of such events may cause decomposition, resulting in seafloor leakage of methane. Therefore, the methane flux at the bottom of site SH1 may be affected by the decomposition of natural gas hydrate at the bottom of site SH3. Therefore, the SMTZ distribution is obviously deeper than that at site SH3. This conclusion is consistent with the fact that the SMTZ is relatively shallow when the methane flux is relatively large.

Site SH3 is the most complex of the three sites, and it is difficult to determine whether the deposition rate or the methane flux dominates the movement of the SMTZ. However, the detailed study of the Ba peak is conducive to the understanding of its basic situation. In general, diagenetic front composed of labile Ba exists in shallow sediments above the paleo-SMTZ and the current SMTZ of site SH3. Simple calculations demonstrate that these Ba fronts were formed in the past. The minimum time required to precipitate a Ba front can be estimated from the quantity of Ba in the front and the supply of Ba to the front. At site SH3, the total area concentration of the double Ba front above the paleo-SMTZ is 16.867×10^{-6}; however, the value of the double Ba front at the current SMTZ is 32.98×10^{-6}.The downward supply of solid Ba determines the minimum time required to generate the Ba in a front. The average concentrations of solid Ba above and below the front at the paleo-SMTZ at site SH3 were 380×10^{-6} and 400×10^{-6}, respectively (Fig. 7), indicating a net loss of 20×10^{-6} Ba as solid particles are buried through the SO_4^{2-}/CH_4 interface. The average concentrations of solid Ba above and below the front at the current SMTZ of site SH3 are 450×10^{-6} and 523×10^{-6}, respectively (Fig. 7), indicating a net loss of 73×10^{-6} Ba as solid particles are buried through the SO_4^{2-}/CH_4 interface. The average sediment porosity and grain density of sediment at site SH3 are 40% and 2.6 g/cm^3, respectively (Jin et al, 2019). With a sedimentation rate of 13 cm/ka, the time required to form the Ba front at the top of the paleo-SMTZ was about 2 times required to form the Ba

front at the bottom of the current SMTZ. Therefore, the formation time of the SMTZ was longer than that of the paleo-SMTZ. In fact, double Ba peaks appeared at the top of the paleo-SMTZ and current SMTZ of site SH3, indicating that the SMTZ of these two periods was not stable but rather was in a process of moving slowly.

5.4 *Relationship between movement of the SMTZ and methane leakage and debris input*

At site 973-4, the SMTZ also showed a tendency to move vertically. However, the mechanism of the movement at site 973-4 was significantly different from that of the modern SMTZ of site SH3. At site 973-4, the TOC/TN ratio did not change from the shallow portion to the deep portion, indicating that the input of the detrital material was stable; however, the result showed a significant decrease at the top of the SMTZ. The carbonate and Ba contents also decreased significantly. Xie et al (2019) believed that the geological time at the top of the SMTZ of site 973-4 was during the last glacial maximum, when there was an obvious contour current deposition rate of 91 cm/ka. However, Fe_2O_3 and Al_2O_3 did not increase. Shao et al (2007) analysed many seismic sections in the northern part of the SCS and discovered the existence of contour current flow at the bottom of site 973-4. The contour current deposition at the bottom of the seabed was the main reason for the high rate of deposition of the sediment. The high sedimentation rate deposits caused the SMTZ to move downward quickly, made the biogenetic barite unstable and diluted the carbonate in the sediment. The high sedimentation rate sediments are also the main reason for the reducing environment of site 973-4. The clear enrichment of U–Mo at the top of the SMTZ indicates a closed reducing depositional environment. At the same time, the primary productivity at the top of the SMTZ was also significantly reduced because both Cu/Al and Ni/Al were significantly negative (Figs 3c and d). Thus, the contour current deposition had an important influence on the formation of the submarine sedimentary environment, the movement of the SMTZ, and the enrichment of elements.

At site SH1, the indices of detrital materials of Ti, Al, and Fe all decreased at the SMTZ (Fig. 6). In the paleo-SMTZ layer at site SH3, the sedimentary environment was very similar to that of site 973-4, a closed reducing sedimentary environment, and the indicators of terrestrial debris in the paleo-SMTZ layer were obviously increased. However, the difference of site 973-4 is that the input of TDM at the paleo-SMTZ of site SH3 was not very high, only 20 cm/ka (Hsu et al, 2014), so the migration of the SMTZ was relatively slow and enriched carbonate and pyrite formed. The Ba in this layer exhibits a double peak, which also confirms the slow movement of its SMTZ from the side. It is foreseeable that it may hardly find any signs of an SMTZ in a depositional environment with a high deposition rate but low methane flux because the rapidly moving SMTZ is not conducive to the formation of the various minerals and the occurrence of the related chemical reactions (Lu et al, 2017).

The SMTZ at site SH3 in the Shenhu area was the most stable. Hence, the AOM signal in its sediment was the strongest. This reduced input of terrigenous detrital materials was conducive to improvement of primary productivity. At the modern SMTZ, the Cu/Al and Ni/Al ratios at site SH3 were also increased (Figs 3c and j), indicating higher primary productivity. The U–Mo coupling system indicated that the depositional environment of the modern SMTZ was suboxic, and such a depositional environment is very beneficial to microbial activity. Therefore, the input of terrigenous debris is an important influencing factor.

6 Conclusion

This study examined the $\delta^{34}S$, terrigenous clastic indices of TiO_2 and Al_2O_3, and redox indices of U and Mo at site 973-4 in the Taixinan Basin and sites SH3 and SH1 in the Shenhu area. The coupled relationships between the different systems of deposition rates and methane fluxes showed distinctly different manifestations for the distribution of the SMTZ.

(1) At site 973-4, the deposition rate had a dominant role, so the SMTZ, depositional environment, and primary productivity were affected by the high deposition rate. Affected by the high deposition rate, the SMTZ showed a significant downward migration.

(2) At site SH1, the coupled model of deposition rate and methane flux was dominated by methane flux. The result is in accordance with the general understanding that the SMTZ is shallow when the methane flux is large and the SMTZ is deep when the methane flux is small.

(3) At site SH3, the coupled model of deposition rate and methane flux showed that the two aspects are in a process of dynamic equilibrium. Thus, the AOM effect was the most stable. At site SH3, through calculation of the Ba peak, the SMTZ was found to be more stable than the paleo-SMTZ. In this case, the AOM signal in the sediment was the strongest (Fig. 9).

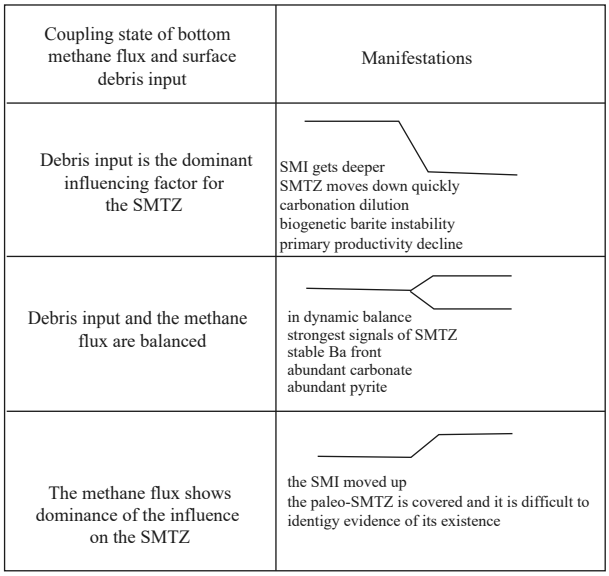

Fig. 9. Different manifestations of the AOM effect in the natural environment attributable to various combinations of methane flux and deposition rate.

Acknowledgements

The samples were collected by the *Haiyang-6* and *GMGS1* Scientific Research Boat of the Guangzhou Marine Geological Survey, China. The authors thank the voyage scientists for their hard work in collecting the research samples. The authors also thank the Guangzhou Institute of Geochemistry CAS for total organic carbon analysis, Wuhan Institute of Science and Technology Co., Ltd. for trace elements analysis, and the Analysis and Testing Center of China University of Geosciences (Wuhan, China) for S isotope tests.

References

Berner R A. 1981. A new geochemical classification of sedimentary environments. Journal of Sedimentary Petrology, 51(2):

359–365
Dickens G R. 2001. Sulfate profiles and barium fronts in sediment on the Blake Ridge: Present and past methane fluxes through a large gas hydrate reservoir. Geochimica et Cosmochimica Acta, 65: 529–543, doi: 10.1016/S0016-7037(00)00556-1
Dickens G R, Owen R M. 1996. Sediment geochemical evidence for an early-middle Gilbert (early Pliocene) productivity peak in the North Pacific Red Clay Province. Marine Micropaleontology, 27: 107–120, doi: 10.1016/0377-8398(95)00054-2
Dong Huaimin, Sun Jianmeng, Zhu Jinjiang, et al. 2019. Developing a new hydrate saturation calculation mode for hydrate-bearing sediments. Fuel, 248: 27–37, doi: 10.1016/j.fuel.2019.03.038
Egger M, Kraal P, Jilbert T, et al. 2016. Anaerobic oxidation of methane alters sediment records of sulfur, iron and phosphorus in the Black Sea. Biogeosciences, 13(18): 5333–5355, doi: 10.5194/bg-13-5333-2016
Egger M, Rasigraf O, Sapart C J, et al. 2015. Iron-mediated anaerobic oxidation of methane in brackish coastal sediments. Environmental Science & Technology, 49(1): 277–283
Feng Dong, Chen Duofu. 2015. Authigenic carbonates from an active cold seep of the northern South China Sea: new insights into fluid sources and past seepage activity. Deep-Sea Research Part II: Topical Studies in Oceanography, 122: 74–83, doi: 10.1016/j.dsr2.2015.02.003
Feng Dong, Qiu Jianwen, Hu Yu, et al. 2018. Cold seep systems in the South China Sea: an overview. Journal of Asian Earth Sciences, 168: 3–16, doi: 10.1016/j.jseaes.2018.09.021
Hsu S K, Chiang C W, Evans R L, et al. 2014. Marine controlled source electromagnetic method used for the gas hydrate investigation in the offshore area of SW Taiwan. Journal of Asian Earth Sciences, 92: 224–232, doi: 10.1016/j.jseaes.2013.12.001
Jin Guangrong, Lei Hongwu, Xu Tianfu, et al. 2019. Seafloor subsidence induced by gas recovery from a hydrate-bearing sediment using multiple well system. Marine and Petroleum Geology, 107: 438–450, doi: 10.1016/j.marpetgeo.2019.05.008
Kotelnikova S. 2002. Microbial production and oxidation of methane in deep subsurface. Earth-Science Reviews, 58(3): 367–395
Leventhal J S. 1983. An interpretation of carbon and sulfur relationships in black sea sediments as indicators of environments of deposition. Geochimica et Cosmochimica Acta, 47(1): 133–137, doi: 10.1016/0016-7037(83)90097-2
Li Niu, Feng Dong, Chen Linying, et al. 2016a. Using sediment geochemistry to infer temporal variation of methane flux at a cold seep in the South China Sea. Marine and Petroleum Geology, 77: 835–845, doi: 10.1016/j.marpetgeo.2016.07.026
Li Niu, Feng Dong, Chen Linying, et al. 2017. Compositions of foraminifera-rich turbidite sediments from the Shenhu area on the northern slope of the South China Sea: implication for the presence of deep water bottom currents. Journal of Asian Earth Sciences, 138: 148–160, doi: 10.1016/j.jseaes.2017.02.010
Li Chengfeng, Hu Gaowei, Zhang Wei, et al. 2016b. Influence of foraminifera on formation and occurrence characteristics of natural gas hydrates in fine-grained sediments from Shenhu area, South China Sea. Science China Earth Sciences, 59(11): 2223–2230, doi: 10.1007/s11430-016-5005-3
Li Li, Wang Hui, Luo Buchiren, et al. 2008. The characterizations and paleoceanographic significances of organic and inorganic carbon in northern South China Sea during past 40 ka. Marine Geology & Quaternary Geology (in Chinese), 28(6): 79–85
Lim Y C, Lin S, Yang T F, et al. 2011. Variations of methane induced pyrite formation in the accretionary wedge sediments offshore southwestern Taiwan. Marine and Petroleum Geology, 28(10): 1829–1837, doi: 10.1016/j.marpetgeo.2011.04.004
Lin S, Hsieh W C, Lim Y C, et al. 2006. Methane migration and its influence on sulfate reduction in the Good Weather Ridge region, South China Sea continental margin sediments. Terrestrial Atmospheric and Oceanic Sciences, 17: 883–902, doi: 10.3319/TAO.2006.17.4.883(GH)
Lin Zhiyong, Sun Xiaoming, Lu Yang, et al. 2017. The enrichment of heavy iron isotopes in authigenic pyrite as a possible indicator of sulfate-driven anaerobic oxidation of methane: insights from the South China Sea. Chemical Geology, 449: 15–29, doi: 10.1016/j.chemgeo.2016.11.032
Lin Zhiyong, Sun Xiaoming, Lu Yang, et al. 2018. Iron isotope constraints on diagenetic iron cycling in the Taixinan seepage area, South China Sea. Journal of Asian Earth Sciences, 168: 112–124, doi: 10.1016/j.jseaes.2018.01.007
Liu Xiaoyu, Feng Xiuli, Sun Yongfu, et al. 2019. Acoustic and biological characteristics of seafloor depressions in the North Yellow Sea Basin of China: Active fluid seepage in shallow water seafloor. Marine Geology, 414: 34–46, doi: 10.1016/j.margeo.2019.05.002
Liu Tieshu, He Shibin. 2001. Deepwater hydrocarbon potential along the north continental margin, the South China Sea. China Offshore Oil and Gas (Geology) (in Chinese), 15(3): 164–170
Liu Jiarui, Izon G, Wang J, et al. 2018. Vivianite formation in methane-rich deep-sea sediments from the South China Sea. Biogeosciences, 15(20): 6329–6348, doi: 10.5194/bg-15-6329-2018
Liu Weiguo, Wang Zheng, Li Xiangzhong. 2016. The contribution of aquatic plants to sedimentary *n*-alkanes δ^{13}c values using to qualify compositions of terrigenous plants in lake Qinghai on the northeastern Qinghai-Tibetan Plateau. Quaternary Sciences (in Chinese), 36(3): 623–629
Lloyd K G, Lapham L, Teske A. 2006. An anaerobic methane-oxidizing community of ANME-1b archaea in hypersaline Gulf of Mexico sediments. Applied and Environmental Microbiology, 72(11): 7218–7230, doi: 10.1128/AEM.00886-06
Lu Yang, Liu Yufei, Sun Xiaoming, et al. 2017. Intensity of methane seepage reflected by relative enrichment of heavy magnesium isotopes in authigenic carbonates: A case study from the South China Sea. Deep-Sea Research Part I: Oceanographic Research Papers, 129: 10–21, doi: 10.1016/j.dsr.2017.09.005
Panieri G, Bünz S, Fornari D J, et al. 2017. An integrated view of the methane system in the pockmarks at Vestnesa Ridge, 79°N. Marine Geology, 390: 282–300, doi: 10.1016/j.margeo.2017.06.006
Sato H, Hayashi K I, Ogawa Y, et al. 2012. Geochemistry of deep sea sediments at cold seep sites in the Nankai Trough: insights into the effect of anaerobic oxidation of methane. Marine Geology, 323–235: 47–55
Shao Lei, Li Xuejie, Geng Jianhua, et al. 2007. Deep water bottom current sedimentation in the northern South China Sea. Science in China Series D (in Chinese), 50(7): 1060–1066, doi: 10.1007/s11430-007-0015-y
Su Zheng, He Yong, Wu Nengyou, et al. 2012. Evaluation on gas production potential from laminar hydrate deposits in Shenhu Area of South China Sea through depressurization using vertical wells. Journal of Petroleum Science and Engineering, 86–87: 87–98, doi: 10.1016/j.petrol.2012.03.008
Su Ming, Hsiung Kanhsi, Zhang Cuimei, et al. 2015. The linkage between longitudinal sediment routing systems and basin types in the northern South China Sea in perspective of source-to-sink. Journal of Asian Earth Sciences, 111: 1–13, doi: 10.1016/j.jseaes.2015.05.011
Su Ming, Xie Xinong, Wang Zhenfen, et al. 2016. Sedimentary evolution of the Central Canyon System in the Qiongdongnan Basin, northern South China Sea. Petroleum Research, 1: 81–92, doi: 10.1016/S2096-2495(17)30033-9
Tong Hongpeng, Feng Dong, Cheng Hai, et al. 2013. Authigenic carbonates from seeps on the northern continental slope of the South China Sea: new insights into fluid sources and geochronology. Marine and Petroleum Geology, 43: 260–271, doi: 10.1016/j.marpetgeo.2013.01.011
Wang Changkun. 2013. The magnetic parameters and its environmental implications in sediments since late Pleistocene from Dongsha area, South China Sea (in Chinese). Beijing: China University of Geosciences
Wang Jiaze, Li Anchun, Xu Kehui, et al. 2015. Clay mineral and grain size studies of sediment provenances and paleoenvironment evolution in the middle Okinawa Trough since 17 ka. Marine Geology, 366: 49–61, doi: 10.1016/j.margeo.2015.04.007

Wankel S D, Adams M M, Johnston D T, et al. 2012. Anaerobic methane oxidation in metalliferous hydrothermal sediments: influence on carbon flux and decoupling from sulfate reduction. Environmental Microbiology, 14(10): 2726–2740, doi: 10.1111/j.1462-2920.2012.02825.x

Wu Daidai, Xie Rui, Liu Jie, et al. 2020. Zone of metal-driven anaerobic oxidation of methane is an important sink for phosphorus in the Taixinan Basin, South China Sea. Marine Geology, 427: 106268, doi: 10.1016/j.margeo.2020.106268

Wu Nengyou, Yang Shengxiong, Wang Hongbin, et al. 2009. Gas-bearing fluid influx sub-system for gas hydrate geological system in Shenhu Area, northern South China Sea. Chinese Journal of Geophysics (in Chinese), 52(6): 1641–1650

Wu Nengyou, Zhang Haiqi, Yang Shengxiong, et al. 2011. Gas hydrate system of Shenhu area, northern South China Sea: geochemical results. Journal of Geological Research, 2011: 370298

Xie Rui, Wu Daidai, Liu Jie, et al. 2019. Evolution of gas hydrates inventory and anaerobic oxidation of methane (aom) after 40 ka in the Taixinan Basin, South China Sea. Deep-Sea Research Part I: Oceanographic Research Papers, 152: 103084, doi: 10.1016/j.dsr.2019.103084

Yao Bochu. 1996. Tectonic characterictics and evolution of the Nansha Trough. Gresearch of Eological South China Sea (in Chinese), (8): 1–13

Zhang Jie, Lei Huaiyan, Chen Yong, et al. 2018a. Carbon and oxygen isotope composition of carbonate in bulk sediment in the southwest Taiwan Basin, South China Sea: methane hydrate decomposition history and its link to mud volcano eruption. Marine and Petroleum Geology, 98: 687–696, doi: 10.1016/j.marpetgeo.2018.08.031

Zhang Jie, Lei Huaiyan, Yang Ming, et al. 2018b. The interactions of P-S-Fe in sediment from the continental slope of northern South China Sea and their implication for the sulfate-methane transition zone. Earth Science Frontiers (in Chinese), 25: 285–293

Zhang Shengyin, Li Shuanglin, Dong Heping, et al. 2013. Distribution and source identification of polycyclic aromatic hydrocarbon of surface sediments from the center part of South Yellow Sea, China. China Environmental Science (in Chinese), 33(7): 1263–1270

Zhang Wei, Liang Jinqiang, Lu Jing'an, et al. 2017. Accumulation features and mechanisms of high saturation natural gas hydrate in Shenhu Area, northern South China Sea. Petroleum Exploration and Development, 44(5): 708–719, doi: 10.1016/S1876-3804(17)30082-4

Zhang Weiyan, Zhang Fuyuan, Chen Ronghua, et al. 2002. Constituents of matter and sedimentation fluxes and sedimentation rates of deep-water sedimentation during the late pleistocene in the South China Sea. Acta Sedimentologica Sinica (in Chinese), 20(4): 668–674

Zhao Shaohua, Liu Zhifei, Chen Quan, et al. 2017. Spatiotemporal variations of deep-sea sediment components and their fluxes since the last glaciation in the northern South China Sea. Science China: Earth Sciences, 60(7): 1368–1381, doi: 10.1007/s11430-016-9058-6

Zheng Guodong, Xu Wang, Etiope G, et al. 2018. Hydrocarbon seeps in petroliferous basins in China: a first inventory. Journal of Asian Earth Sciences, 151: 269–284, doi: 10.1016/j.jseaes.2017.10.037